Dai, P., Yang, L., Wang, J. and Zhou Y. (2019). Compressive strength of concrete-filled stainless steel tube stub columns. Engineering Structures, accepted.

Compressive strength of concrete-filled stainless steel tube stub columns

Peng Dai[a,b], Lu Yang[a,b,*], Jie Wang[c], Yuhang Zhou[a,b]

[a]*The Key Laboratory of Urban Security and Disaster Engineering of Ministry of Education, Beijing University of Technology*, *Beijing 100124, China*

[b]*Beijing Engineering Research Centre of High-rise and Large-span Prestressed Steel Structures, Beijing University of Technology*, *Beijing 100124, China*

[c]*Department of Architecture and Civil Engineering, University of Bath, Bath BA2 7AY, UK*

Abstract. Concrete-filled stainless steel tube (CFSST) members combine the advantages of the outstanding corrosion resistance of stainless steel and the composite action in concrete-filled steel tube (CFST) system. However, accurate calculation methods for this type of structures are currently limited and research into CFSST members with hot-rolled stainless steel tubes are not available. In this paper, the compressive behavior of CFSST stub columns has been investigated through a comprehensive experimental and numerical program. A total of 18 specimens, including 9 concrete-filled austenitic stainless steel tube (austenitic CFSST) and 9 concrete-filled duplex stainless steel tube (duplex CFSST) stub columns, were tested under compression. The varying parameters in the experimental study included the thickness of the stainless steel tube and the strength of the concrete. Finite element (FE) models duplicating the tests were developed, which were subsequently used in a parametric study to generate a wider range of data and to investigate the influence of the tube thickness and concrete strength on the ultimate capacities of CFSST stub columns. Based on the generated data, it was found that the current European and Chinese standards for concrete-filled carbon steel tubes underestimate the resistances of CFSST members significantly. To this end, new calculation methods developed based on these European and Chinese design rules have been proposed, which were shown to provide improved strength predictions for both the austenitic and duplex CFSST members.

Keywords: Axial compression; Calculation methods; Composite members; Concrete-filled stainless steel tubes; Experimental tests; Parametric study; Stub columns

1. Introduction

Concrete-filled steel tube (CFST) members have been extensively applied in the building industry due to high strength, excellent ductility and earthquake-resistant performance [1 – 3]. However, the traditional CFST members used in high-rise buildings and long-span bridges have been proved to suffer from reduced durability due to corrosion problems, resulting in high maintenance costs. Having the advantages of high corrosion resistance, aesthetic appearance and fire resistance, stainless steels can reduce the maintenance cost as the members can be directly exposed to the environment without protective coatings. To this end, an alternative design, concrete-filled stainless steel tube (CFSST) members combining the high corrosion resistance of stainless steel with the advantages of CFST system, is considered as a promising solution. Despite the fact that both CFST and CFSST systems rely on the constraint effect, the change of conventional carbon steel in CFST to stainless steel in CFSST member results in significantly different resistance due to the difference in their material properties, and the CFSST members should not be designed with the same set of equations as for the CFST members.

There has been a large number of studies on CFST members [4-10], where the local and global buckling resistances of the system have been systematically investigated and the corresponding design methods have been proposed. In contrast, the study of CFSST members has only started recently. Han et al. [11] reviewed recent studies on the behavior of CFSST members and discussed future research directions of CFSST system. Lam and Gardner [12] studied experimental behavior of CFSST columns under compression and have found that existing calculation methods for CFST members are overly conservative when applied to CFSST. Young and Ellobody [13] tested concrete-

filled cold-formed stainless steel tube columns under axial compression and proposed design recommendations for cold-formed CFSST columns. Dabaon et al. [14] conducted a number of stiffened and unstiffened CFSST column tests under compression and have found that the stiffened members offered higher confinement of the concrete core than the unstiffened ones. Tao et al. [15], Uy et al. [16] and He et al. [17] carried out studies on CFSST stub columns under axial compression and proposed design methods based on current CFST design provisions. Other structural aspects of CFSST members, i.e. the bond-slip, flexural, and fire-resistant behaviors, were investigated in Chen et al. [18, 19] and Ellobody [20], respectively. It should be noted that these previous research mainly focused on the CFSST members with cold-formed thin-walled stainless steel tubes and very few have focused on hot-rolled members with relatively thick tube section walls. Compared with cold-formed steel sections, hot-rolled sections have more homogeneous material properties, consistent hardness, better ductility and relatively lower residual stresses. The wall thickness of hot-rolled sections is in general larger than cold-formed steel tubes, thereby providing better restraints to the concrete core. Therefore, the CFSST members with hot-rolled stainless steel tubes are likely to possess higher structural efficiency than those with cold-formed steel tubes. As the most commonly used types of stainless steels, austenitic and duplex stainless steels are focused in the current study.

In addition to the fact that there is very few study on the behavior of CFSST members with hot-rolled stainless steel tubes, there is also a scarce of corresponding design regulation. To this end, in the present study, 18 CFSST specimens made of hot-rolled austenitic or duplex stainless steel tubes were tested under compression to study their compressive bearing capacities. Finite element (FE) models were established and validated against the experimental results, and subsequently used for a comprehensive parametric study taking into account a wider range of geometric parameters. Based on the data of the parametric analysis, calculation methods for the compressive strength of CFSST

stub columns were proposed on the basis of the traditional CFST design formulae in the Chinese and the European design standards for composite structures.

2. Experimental program

2.1 Test specimens

The specimens in the current study covered six cross-section geometries (CHS 300×8, 300×10 and 300×12 in AISI 304 stainless steel and CHS 325×8, 325×10 and 325×12 in AISI 2205 stainless steel) and three concrete grades, giving a total of 18 specimens, as listed in Table 1. In the specimen label designation in Table 1, the 304 or 2205 refers to the grade of the stainless steel, the number after the letter t stands for the nominal thickness (in mm) of the steel tube, and the number after the letter c represents the cube compressive strength (in MPa) of the concrete. During the preparation of each specimen, prior to casting the concrete, a Q235 carbon steel plate was welded onto one end of the steel tube adopting E-309 or E-2209 welding rods for the 304 and 2205 material, respectively. The concrete was then poured and the specimens were compacted in a vibration table. Twenty-eight days after curing the concrete, the high-strength mortar was used to fill in the gap caused by the shrinkage of the concrete. The casted CFSST stub columns were then covered by welding a carbon steel plate onto the other end. Figs. 1(a) and (b) show the side and plan view of the fabricated CFSST specimens, respectively.

The geometric dimensions and material properties of each specimen are reported in Table 1, where D, t and L are the outer diameter, thickness and length between the inner side of the endplates, respectively, of the stainless steel tube, $f_{0.2}$ is the yield strength (0.2% proof strength) of the stainless steel as obtained from the tensile coupon tests, f_{cu} is the cube compressive strength of the concrete, ξ is the confinement factor defined as $\xi = A_s f_{0.2}/A_c f_{ck}$, with A_s and A_c being the cross-sectional areas of the stainless steel tube and the concrete core, respectively, and f_{ck} being the characteristic compressive strength of concrete calculated as $0.67f_{cu}$ according to EN 1992-1-1 [21, 22]. It should

96 be noted that all the stub columns were designed with a length of $L = 3D$ to avoid premature
97 occurrence of global instability and to ensure local buckling failure modes.

Table 1 List of CFSST stub column specimens

Specimen label	D (mm)	t (mm)	L (mm)	$f_{0.2}$ (MPa)	f_{cu} (MPa)	ξ
304-t8c40	298.45	7.74	900.20	248	40.0	1.04
304-t10c40	299.00	9.89	898.60	242	40.0	1.37
304-t12c40	297.56	11.85	902.10	249	40.0	1.70
304-t8c44	299.00	7.74	900.60	248	44.3	0.95
304-t10c44	299.00	9.89	899.20	242	44.3	1.26
304-t12c44	297.65	11.87	900.00	249	44.3	1.57
304-t8c48	298.52	7.76	900.00	248	47.7	0.89
304-t10c48	298.45	9.87	900.40	242	47.7	1.19
304-t12c48	298.28	11.89	899.20	249	47.7	1.47
2205-t8c43	323.22	7.88	975.00	544	43.0	2.03
2205-t10c43	324.00	9.85	973.20	542	43.0	2.63
2205-t12c43	323.25	11.92	976.50	542	43.0	3.32
2205-t8c50	323.22	7.88	975.10	544	50.0	1.80
2205-t10c50	323.00	9.89	974.60	542	50.0	2.33
2205-t12c50	324.50	11.94	974.60	542	50.0	2.94
2205-t8c54	325.00	7.85	975.20	544	53.8	1.67
2205-t10c54	324.20	9.90	973.40	542	53.8	2.16
2205-t12c54	324.31	11.94	975.50	542	53.8	2.73

Table 2 Measured material properties of the stainless steels

Steel type	t (mm)	$f_{0.2}$ (MPa)	f_u (MPa)	E_0 (MPa)	ε_u (%)	ε_f (%)	n
Austenitic	8	248	633	193250	55.6	61.8	6.4
	10	242	634	198350	52.4	61.8	5.8
	12	249	603	208420	52.5	61.2	6.3
Duplex	8	544	725	192330	22.8	41.6	5.7
	10	542	719	201220	21.2	41.6	6.1
	12	542	724	199540	21.1	39.7	6.2

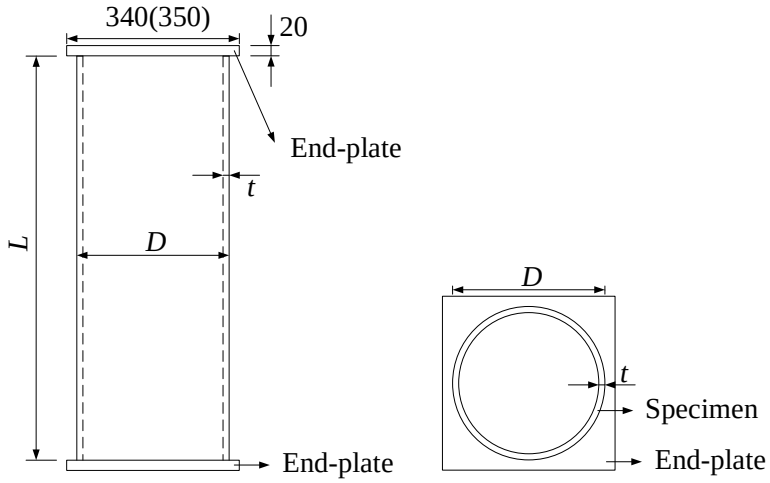

(a) Side view (b) Plan view

Fig.1 Schematic views of CFSST specimens and notations of dimensions

2.2 Material tests

The tensile coupon tests were executed for all the six transverse dimensions (3 in austenitic and 3 in duplex stainless steel). For each cross-section, 3 coupons were extracted from the tube along the rolling direction, giving a total of 18 coupons. The tensile coupon tests were conducted following the EN ISO 6892-1 [23] specified procedure. Typical measured stress-strain relationships of the 304 and 2205 tubes with different thicknesses are shown in Figs. 2(a) and (b), respectively, with both steel grades displaying round-shaped curves as expected for stainless steel materials. The averaged values of key material properties are given in Table 2, where E_0 is Young's modulus, f_u is the ultimate stress, ε_u is the strain at the ultimate stress, ε_f is the plastic strain at fracture and n is the Ramberg-Osgood strain hardening exponent [24].

The cube strength tests were conducted for the poured concrete, where the cubes were cured in an identical environment as for the concrete in the CFSST specimens and tested at 28 days after curing. Since the cube specimens were 100 × 100 × 100 mm^3 cubes, the obtained cube strength $f_{cu,100}$ was translated to the 150 mm cube compressive strength $f_{cu} = 0.95f_{cu,100}$ according to GB/T 50081-2002 [25]. In total there were 6 batches of the poured concrete with 3 cubes being made for each batch.

The obtained averaged cube strength f_{cu} for each batch is reported in Table 1.

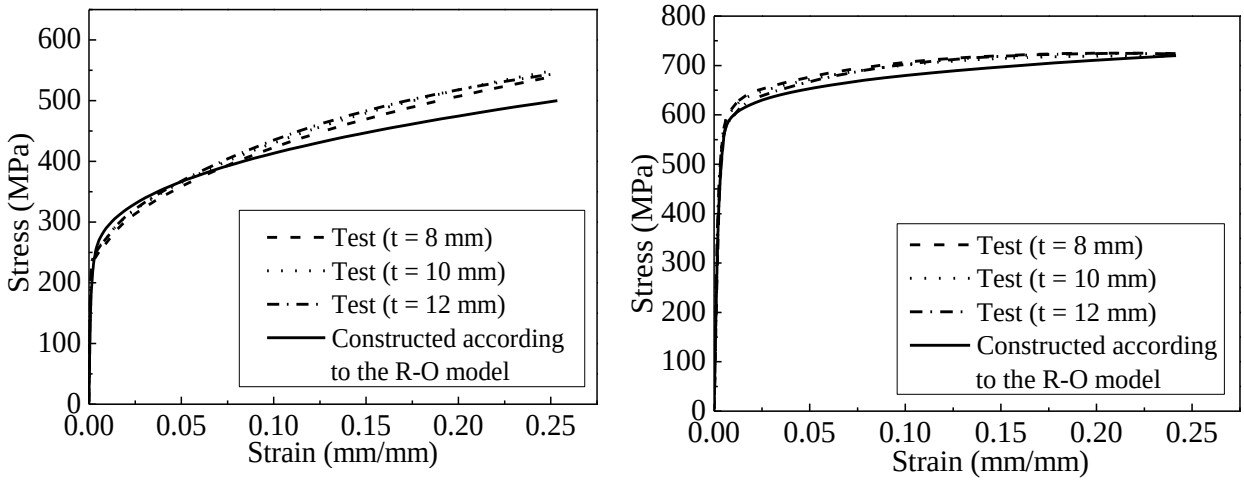

(a) 304 steel (b) 2205 steel

Fig. 2 Stress-strain curves of the stainless steels

2.3 Stub column test setup

An illustration of the test set-up is given in Fig. 3. The specimens were loaded at the top with a pinned condition and fixed supported at the bottom. A graded loading method was adopted in all the tests, which included an initial load control at a speed of 200 kN/min and pauses at every 1000 kN, and a displacement control at a speed of 1 mm/min after the load vs end-shortening curve entered the plastic stage. The tests were terminated when the end-shortening displacement reached approximately 160 and 80 mm respectively for the 304 and 2205 CFSST stub columns. Some tests were terminated earlier before reaching the specified displacements due to safety reasons. Nevertheless, all the tests have achieved deformations where obvious local buckling of the stainless steel tubes have occurred.

During the tests, the applied load, longitudinal end-shortening, longitudinal and transverse strains were monitored. The longitudinal end-shortening was recorded using 4 linear variable displacement transducers (LVDTs) with LVDTs 1 and 2 placed diagonally at the bottom loading plate and LVDTs

3 and 4 at the top. The longitudinal and transverse strains were measured by 4 pairs of strain gauges arranged at 90 degree intervals circumferentially at the mid-height cross-section (Fig. 3(c)) and 2 pairs of strain gauges at 180 degree intervals at the sections 1-1 and 3-3 that were 70 mm away from each end (Fig. 3(d)).

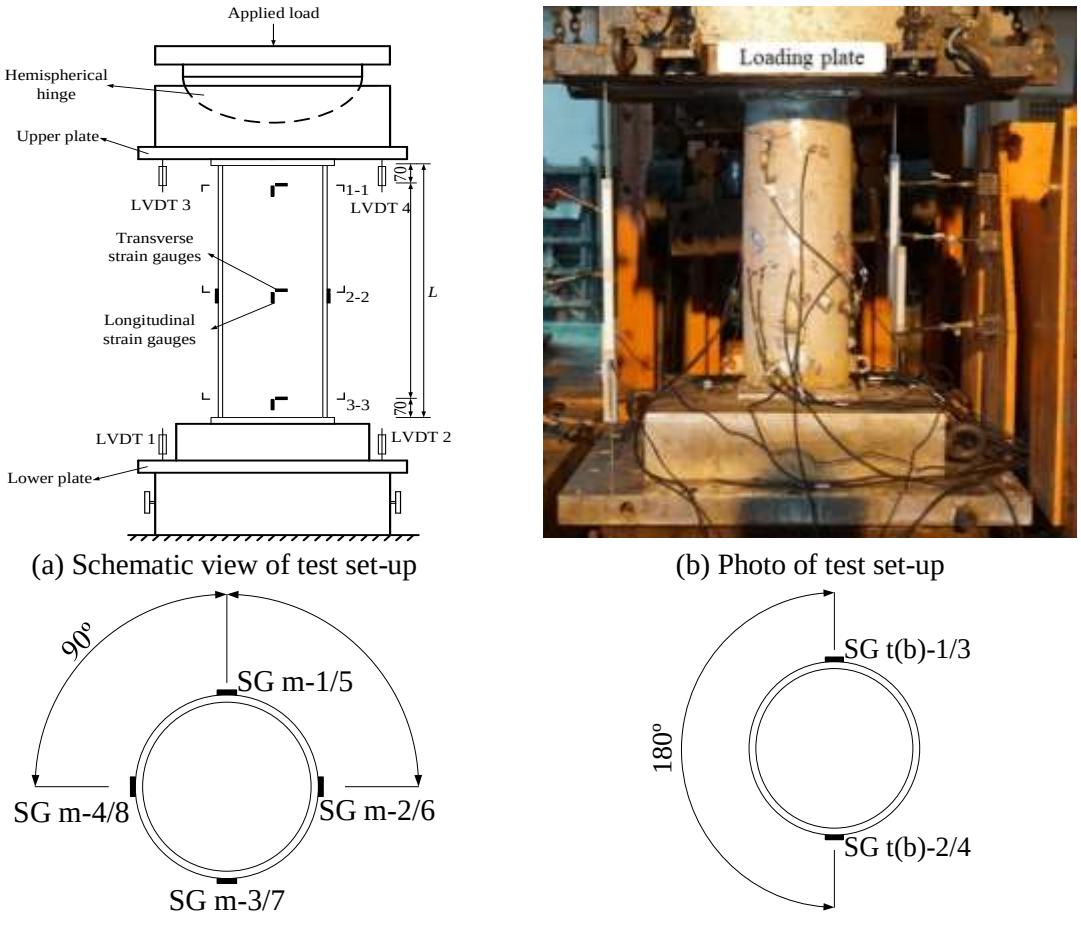

(a) Schematic view of test set-up

(b) Photo of test set-up

(c) Locations of strain gauges at section 2-2

(d) Locations of strain gauges at sections 1-1 and 3-3

Fig. 3 CFSST stub column test set-up

It should be noted that during the tests, load eccentricities occurred in some specimens due to an internal problem in the loading machine, which was unknown prior to testing. The actual initial eccentricity derived based on the strain gauge readings is reported in Table 3 for each specimen.

This phenomenon was considered in the discussion of test results and is shown later in this paper to be able to be accurately captured by the FE models developed. Although the test results are not strictly representative for the ideal loading case of uniform compression, the final assessment of the behavior and design proposals were developed based on the validated FE data, where the ideal uniform compression loading case was applied. It is concluded herein that the load eccentricities occurred in the tests did not affect the validity of the current study.

Specimen label	Load eccentricity (mm)	$N_{u,e}$ (kN)	$N_{u,FEA}$ (kN)	$N_{u,FEA}$ / $N_{u,e}$
304-t8c40	65.4	4709.6	5000.8	1.062
304-t10c40	88.6	5325.3	5381.4	1.010
304-t12c40	84.5	6064.6	6398.2	1.055
304-t8c44	54.3	4955.5	5308.8	1.071
304-t10c44	87.6	5378.7	5504.1	1.023
304-t12c44	83.4	6154.2	6484.4	1.054
304-t8c48	74.6	4640.4	4936.4	1.064
304-t10c48	86.4	5444.8	5554.3	1.020
304-t12c48	83.5	6224.9	6531.6	1.049
			Mean	1.045
			COV	0.02
2205-t8c43	28.6	10167.4	10320.7	1.015
2205-t10c43	38.4	11016.6	11612.3	1.054
2205-t12c43	26.8	12726.2	13638.6	1.072
2205-t8c50	25.4	10298.8	10620.0	1.031
2205-t10c50	62.4	9729.6	10719.7	1.102
2205-t12c50	41.3	12235.3	13159.2	1.075
2205-t8c54	27.6	10436.7	10733.2	1.028
2205-t10c54	12.0	13200.3	13214.0	1.000
2205-t12c54	24.8	13115.7	13964.0	1.065
			Mean	1.049
			COV	0.03

2.4 Stub column test results

The ultimate loads obtained from the tests are reported in Table 3 and typical failure modes and load

142 vs end-shortening curves are given in Figs. 4 and 5, respectively. In the initial stage of loading, the
143 specimens were bent slightly due to the occurrence of loading eccentricity from the machine. When
144 the end-shortening reached around 10 to 15 mm, the steel tube on the compression side at the
145 specimens' top end bulged out. This was attributed to the fact that the concrete core at this location
146 was crushed. In the later stage of the test, as the deformation continued to develop the bottom end
147 of the specimens also developed a local buckling bulge of the steel tube on the compression side.
148 All the CFSST stub column specimens displayed similar failure modes as shown in Fig. 4, where
149 local buckling occurred on the compression sides of the top and bottom ends of the stainless steel
150 tubes, as induced by a noticeable global curvature caused by the initial load eccentricity. It should
151 be noted that the 304 specimens displayed much larger local buckling bulges and higher degrees of
152 bending and end shortening than the 2205 specimens. This was due to the facts that 1) the 304
153 specimens, in general, had much larger initial eccentricities (Table 3), and 2) the 304 stainless steels
154 are more ductile and possess larger strain-hardening than the 2205 materials (see Table 2) and are
155 able to resist larger deformation before failure.

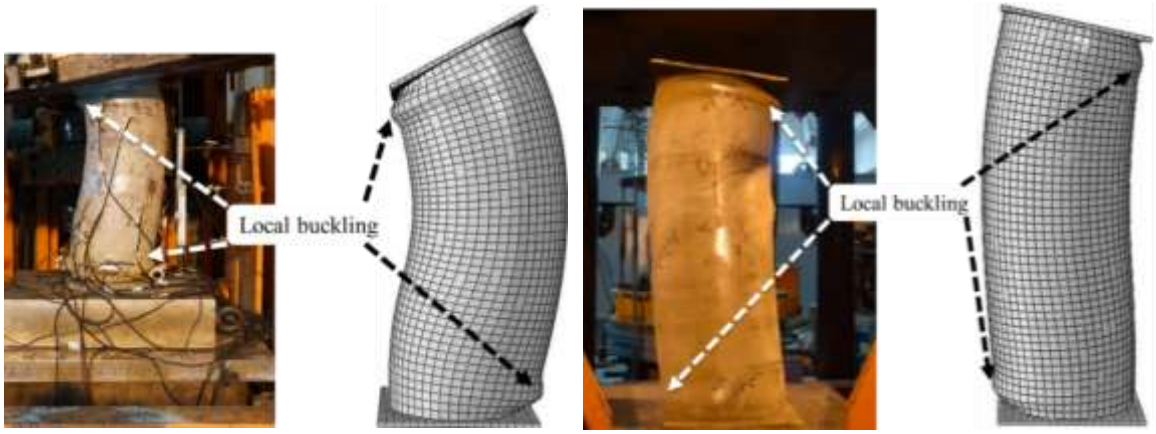

(a) Specimen 304-t8c48 (b) Specimen 2205-t8c54

Fig. 4 Typical failure modes of the CFSST specimens

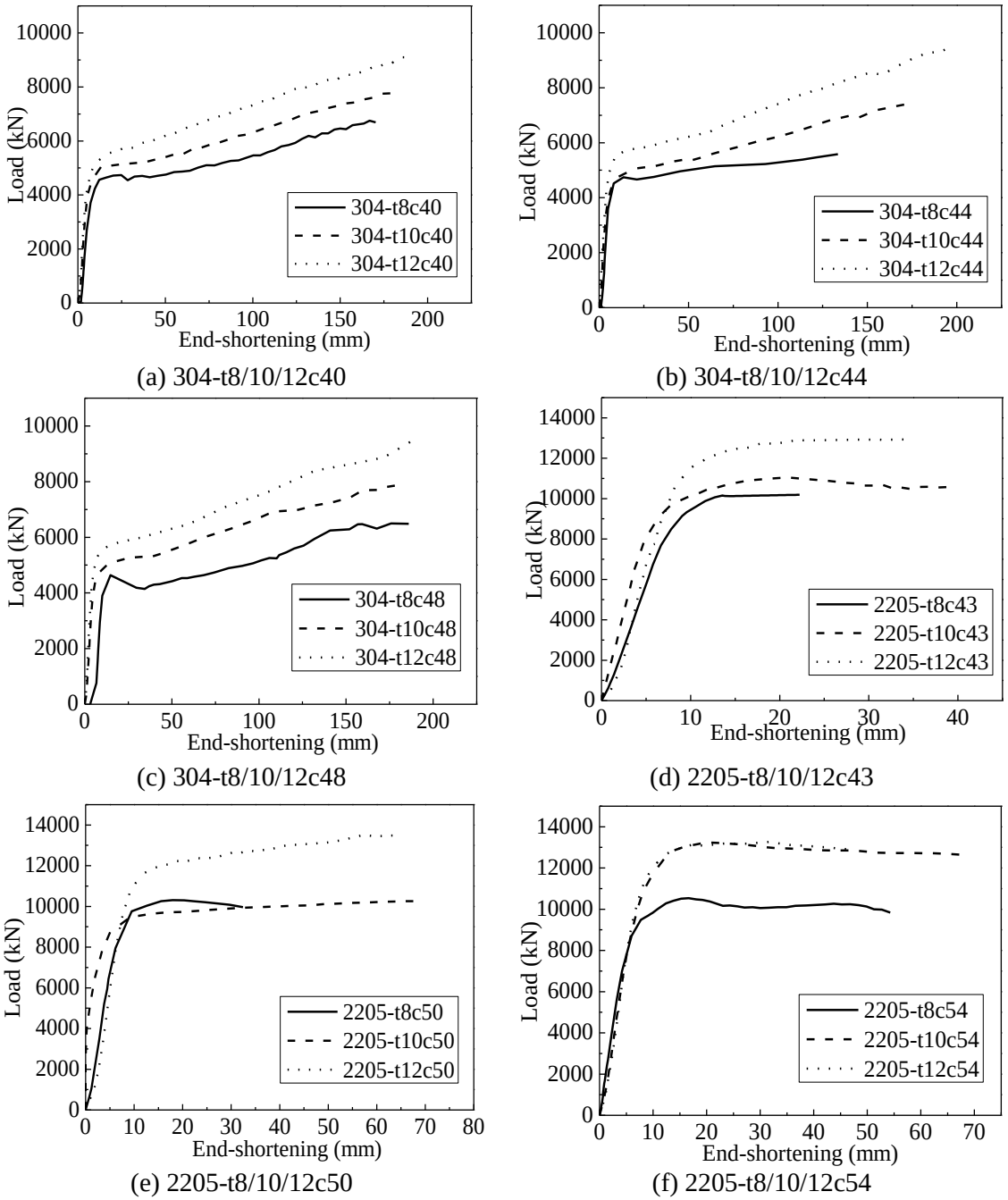

(a) 304-t8/10/12c40 (b) 304-t8/10/12c44

(c) 304-t8/10/12c48 (d) 2205-t8/10/12c43

(e) 2205-t8/10/12c50 (f) 2205-t8/10/12c54

Fig. 5 Load vs end-shortening curves of CFSST stub columns

Fig. 6 depicts the load versus longitudinal and transverse strains relationships of the middle and both ends of the 304-t8c44 and 2205-t10c43 specimens. In the legend designation in Fig. 6, the SG refers

158 to strain gauges, the t, m or b stands for the top, middle or bottom sections of the stainless steel tube,
159 respectively, and the number represents the specific location of the strain gauge according to Fig. 3.
160 In general, in all specimens, the longitudinal strains developed faster than the transverse strains
161 before the peak load was reached. The 304 specimens displayed significant strain-hardening before
162 reaching the peak load (as shown in Figs. 6(a), (c) and (e)), while the 2205 specimens' peak loads
163 occurred quite early and the strain development afterwards did not contribute to a load increase (Figs.
164 6(b), (d) and (f)). Apart from the reason that the 2205 materials in nature are less ductile and process
165 less strain hardening than the 304 materials, this phenomenon is also attributed to the fact that the
166 2205 specimens in this study have much larger cross-section slendernesses than the 304 specimens
167 and are more prone to local buckling. Nevertheless, the stainless steel has reached the yield strain
168 for all specimens before the peak load was attained, demonstrating that the circular stainless steel
169 tubes had a sufficient constraint on the concrete core and the concrete core, in turn, played an
170 important role in restraining the buckling of the stainless steel tube [26]. The relatively large
171 differences between the longitudinal strain gauge readings in all figures of Fig. 6 were mainly
172 attributed to the load eccentricities occurred during the tests.

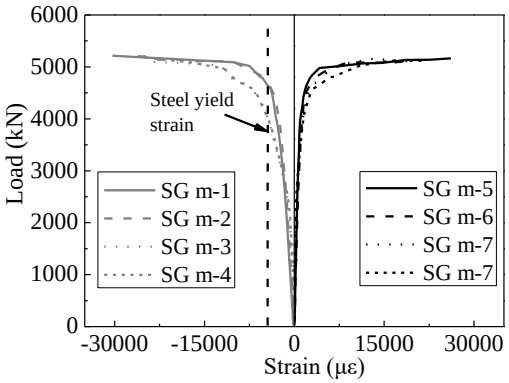

(a) Middle of specimen 304-t8c44

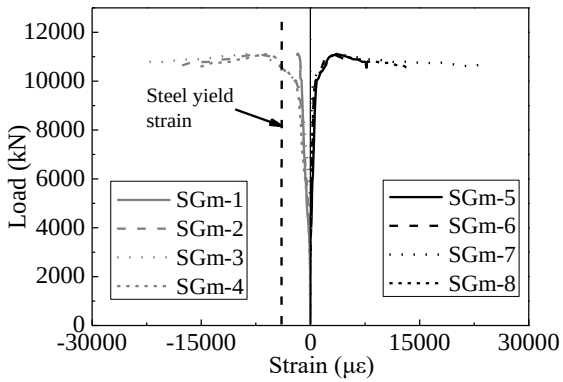

(b) Middle of specimen 2205-t10c43

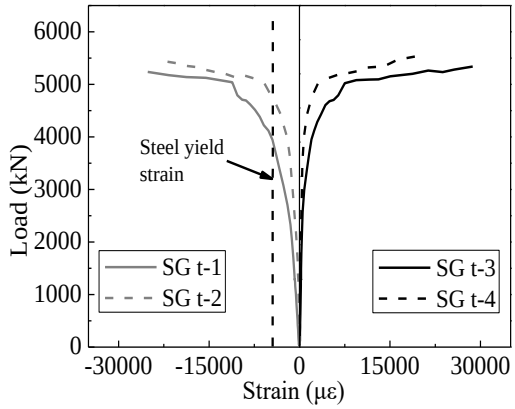

(c) Top of specimen 304-t8c44

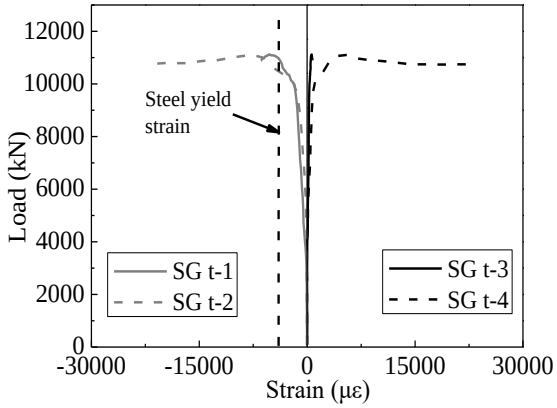

(d) Top of specimen 2205-t10c43

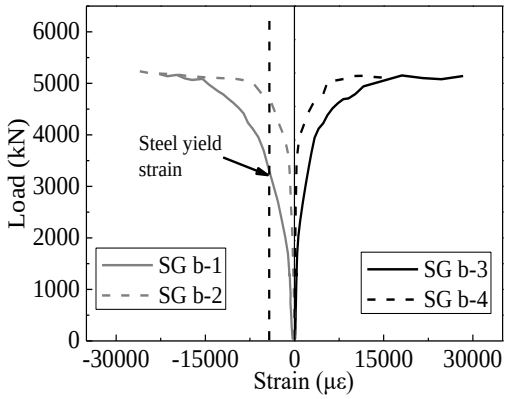

(e) Bottom of specimen 304-t8c44

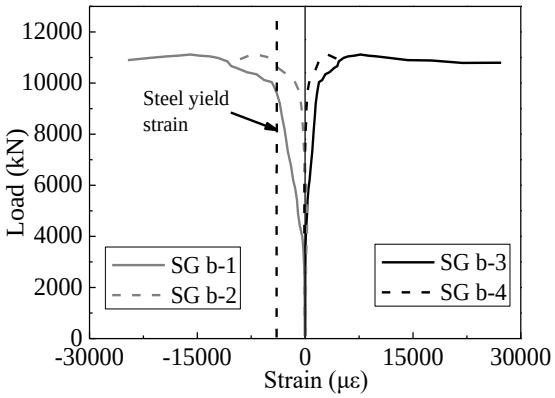

(f) Bottom of specimen 2205-t10c43

Fig. 6 Typical load-strain relationships of 304 and 2205 CFSST stub columns

3. Numerical modeling

In parallel with the test project, a numerical study was conducted to investigate the compression behavior of CFSST stub columns considering a greater range of geometric dimensions. The FE software ABAQUS [27] was adopted throughout the numerical analysis. The modeling assumptions and verification of the finite element models are described in this section, and the subsequent parametric study is detailed in section 4.

3.1 Material modeling of stainless steel tubes

The key material elasticity and plasticity parameters of the stainless steel tubes in the FE models

employed the measured values as reported in Table 2. The stress-strain ($\sigma - \varepsilon$) relationships defining the plasticity in the FE models were represented by the modified R-O material model [28 – 30]:

$$\varepsilon = \begin{cases} \dfrac{\sigma}{E_0} + 0.002\left(\dfrac{\sigma}{\sigma_{0.2}}\right)^n & (\sigma \le \sigma_{0.2}) \\ \dfrac{\sigma - \sigma_{0.2}}{E_{0.2}} + \varepsilon_u\left(\dfrac{\sigma - \sigma_{0.2}}{\sigma_u - \sigma_{0.2}}\right)^m + \varepsilon_{0.2} & (\sigma > \sigma_{0.2}) \end{cases} \quad (1)$$

where $\sigma_{0.2}$ and E_0 are the average 0.2% proof stress and initial elastic modulus, respectively; n is the strain-hardening exponent determined as $n = \ln(20)/\ln(\sigma_{0.2}/\sigma_{0.01})$ with $\sigma_{0.01}$ being the measured 0.01% proof stress; $E_{0.2} = E_0/(1+0.002nE_0/\sigma_{0.2})$ is the tangent elastic modulus when the stress reaches $\sigma_{0.2}$; σ_u is the ultimate stress formulated as $\sigma_{0.2}/\sigma_u = (0.2+185\sigma_{0.2}/E_0)/(1-0.0375(n-5))$ [24]; $\varepsilon_{0.2}$ and ε_u are the strain at 0.2% proof stress and ultimate strain, calculated as $\varepsilon_{0.2} = \sigma_{0.2}/E_0 + 0.002$ and $\varepsilon_u = 1 - \sigma_{0.2}/\sigma_u$, respectively; m is calculated as $m = 1+3.5\sigma_{0.2}/\sigma_u$. Comparisons between the constructed $\sigma - \varepsilon$ relationships using Eq. (1) with the tensile coupon test results are given in Figs. 2(a) and (b) for the 304 and 2205 stainless steel, respectively, indicating good representations of the actual material responses of the considered stainless steel materials using the R-O model. The R-O predicted material curves in Fig. 2 were drawn by considering averaged values from the three thicknesses considered (t = 8, 10 and 12 mm).

Before being incorporated into the FE models, the R-O stress – strain relationships ($\sigma_{nom} - \varepsilon_{nom}$) derived from Eq. (1) were translated into true stress σ_{true} and strain ε_{true} using Eqs (2) and (3), respectively [30-32].

$$\sigma_{true} = \sigma_{nom}(1 + \varepsilon_{nom}) \quad (2)$$

$$\varepsilon_{true} = \ln(1 + \varepsilon_{nom}) \quad (3)$$

3.2 Material modeling of concrete

According to the cubic strength of concrete obtained from the tests, the material model of concrete was established. The elastic response and concrete damaged plasticity behavior were determined

according to the approach described in [27] and [34]. The modulus of elasticity was calculated according to Eq. (4) as recommended in ACI 318 [35]. And the Poisson's ratio was set equal to 0.2. The concrete damaged plasticity model in ABAQUS was used and it mainly consists of three aspects: the plasticity parameters, the compression behavior, and the tensile behavior. The key plasticity parameters included the ratio of the second stress invariant on the tensile meridian to that on the compressive meridian, dilation angle, strain hardening/softening rule, flow potential eccentricity, ratio of the compressive strength under biaxial loading to uniaxial compressive strength (f_{b0}/f_c') and viscosity parameter; these parameters were defined following the approach developed in [27]. The behavior of confined concrete under compression was described by a uniaxial stress-strain curve based on [34], as given by Eq. (5). For the tensile behavior, the crack energy model suggested in [36] was adopted in the FE analyses using Eq. (6). The stress-strain curves describing the tensile and compressive behaviors of the confined concrete in the 2205-t8c43 specimen are plotted in Figs. 7(a) and (b), respectively, for illustration purpose.

$$E_c = 4700\sqrt{f_c'} \tag{4}$$

$$\text{Compressive behavior:} \quad y=\begin{cases} 2x - x^2 & (x \le 1) \\ \dfrac{x}{\beta_0 (x-1)^2 + x} & (x > 1) \end{cases} \tag{5}$$

where $x = \varepsilon/\varepsilon_0$, $y = \sigma/\sigma_0$, ε and σ are the compressive strain and stress, respectively, $\sigma_0 = f_c'$ is the cylinder compressive strength of concrete; $\varepsilon_0 = \varepsilon_c + 800\zeta^{0.2}\times10^{-6}$; $\varepsilon_c = (1300+12.5f_c')\times10^{-6}$; $\beta_0 = (2.36\times10^{-5})^{[0.25+(\zeta-0.5)^7]}(f_c')^{0.5}\times0.5$.

$$\text{Tensile behavior:} \quad y=\begin{cases} 1.2x - 0.2x^6 & (x \le 1) \\ \dfrac{x}{0.31\sigma_p^2 (x-1)^{1.7} + x} & (x > 1) \end{cases} \tag{6}$$

where $x = \varepsilon_t/\varepsilon_p$, $y = \sigma_t/\sigma_p$; ε_t and σ_t tensile strain and stress, respectively; ε_p and σ_p are the strain at peak tensile stress and peak tensile stress, respectively; $\varepsilon_p = 43.1\sigma_p$ ($\mu\varepsilon$); $\sigma_p = 0.26(1.25\ f_c')^{2/3}$.

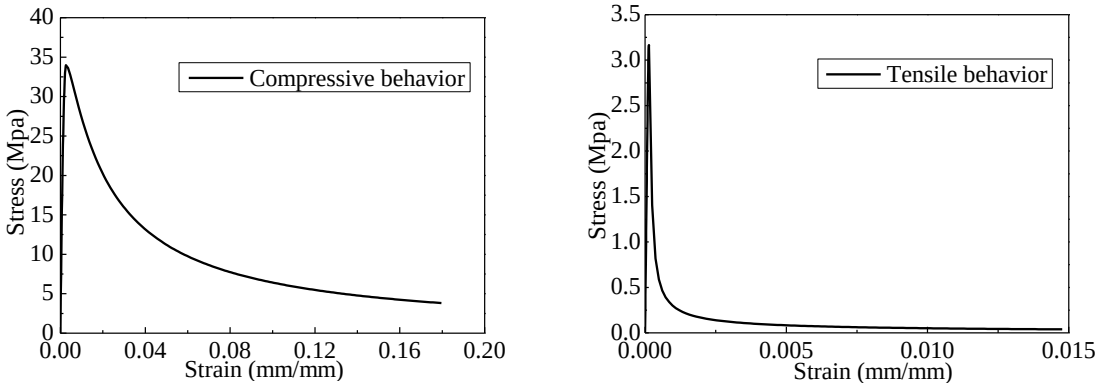

(a) Compressive stress-strain relationship (b) Tensile stress-strain relationship

Fig.7 Stress-strain relationships of the confined concrete in the 2205-t8c43 specimen

3.3 Contact, boundary conditions and load application

The CFSST stub column models were built in the same configuration as in the experiments, where the concrete was housed in the stainless steel tube tied with endplates placed at both ends (see Fig. 8). The contacts between the concrete and the steel tube and between the concrete and the endplates were defined as "hard" contact in the normal direction and a Coulomb friction model [37, 38] in the tangential direction with a friction coefficient of 0.25. The "hard" contact allows the complete transfer of the compressive pressure between the interfaces, and the interfaces are free to separate when there is no compressive pressure.

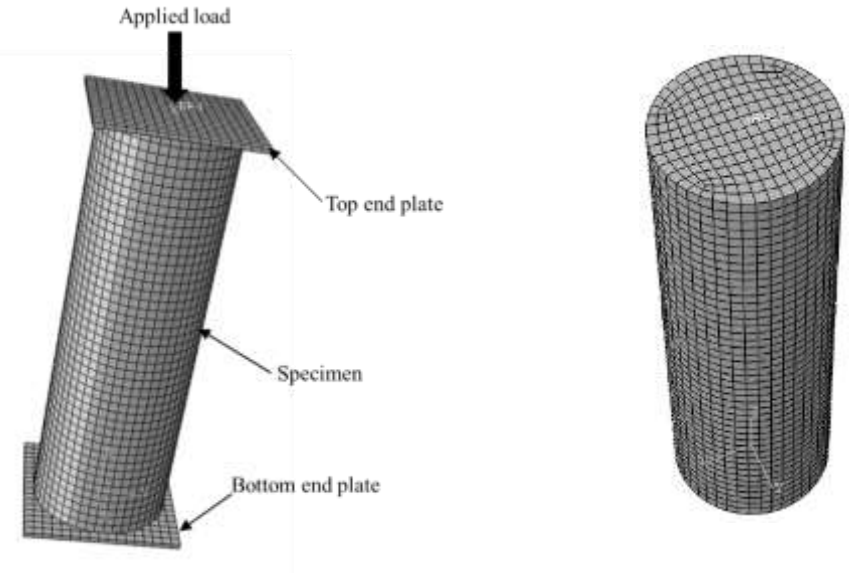

(a) General view (b) Concrete core

Fig.8 Illustration of finite element models

The two endplates were modelled as rigid bodies, tied to the edge of the steel tube at each end. While the bottom endplate was defined with a fixed boundary condition, the top endplate was coupled to a reference point, to which a vertical point load and a pinned boundary condition were applied. The reference point in the FE models duplicating the tests was set at the same height as the centroid of the ball hinge. For tests where load eccentricity occurred, the reference point in the FE model was offset horizontally by the same distance as observed in the test. In the subsequent parametric study, the reference point was set at the centroid of the upper surface of the top endplate.

3.4 Mesh and analysis

The 8-node solid element with reduced integration (C3D8R) was adopted for all parts of the model. A mesh sensitivity study was conducted, concluding that an element size of 20 mm yielded an error within 1%, which was therefore adopted in the models. All the analyses were run with displacement control with Riks algorithm, enabling the post-buckling response to be traced.

3.5 Model validation

Employing the above modeling assumptions, the FE simulations of the 18 CFSST columns in section 2 were carried out. Typical load vs end-shortening curves obtained from the tests and the corresponding FE models are shown in Fig. 9, where consistency between the two has been achieved.

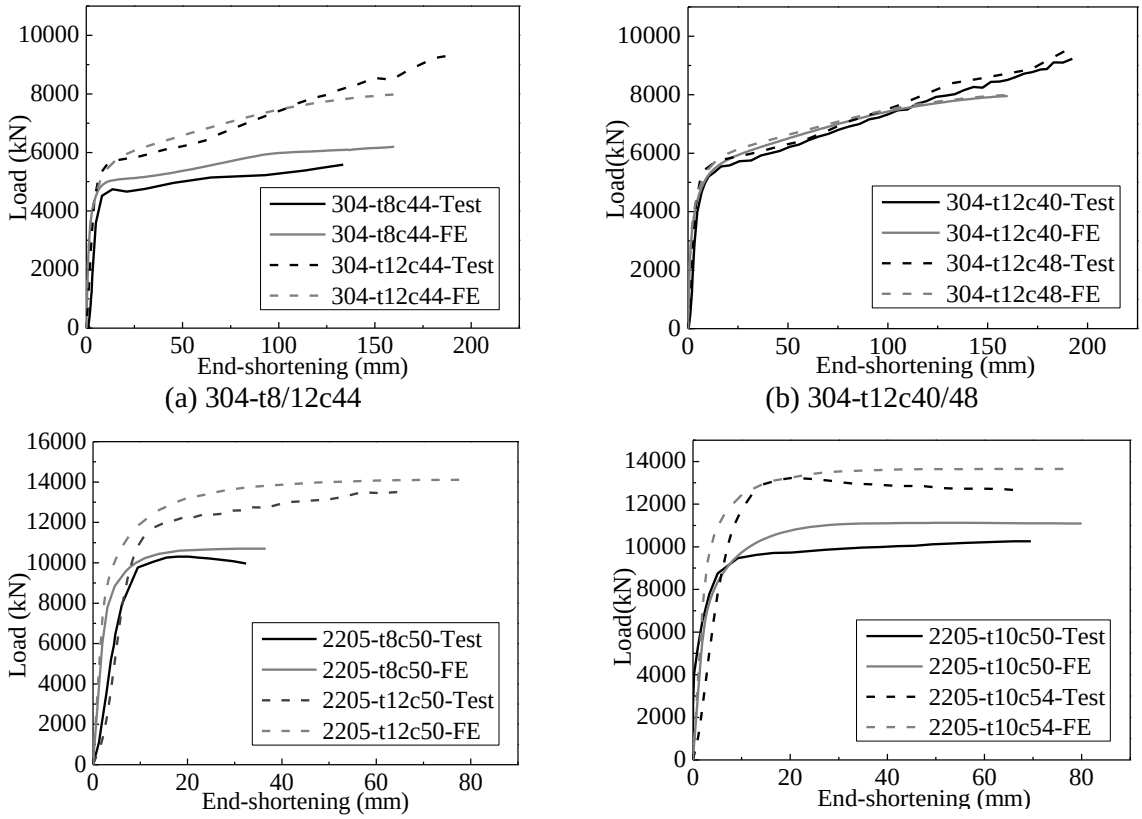

(a) 304-t8/12c44 (b) 304-t12c40/48

(c) 2205-t8/12c50 (d) 2205-t10c50/54

Fig. 9 Typical load vs end-shortening curves of the test and FE CFSST stub columns

Comparisons between the test and FE failure modes for typical specimens (304-t8c48 and 2205-t8c54) are given in Fig. 4, where it can be seen that in both cases the global curvature induced by load eccentricity occurred in the tests can be accurately captured by the FE models. FE simulations of perfectly concentrically loaded CFSST members were also carried out. The typical failure modes are shown in Fig. 10, where *C* stands for the strength grade of the concrete, *D* and *t* represent the diameter and thickness of the outer stainless steel tube, respectively. It can be found that the local

buckling in concentrically loaded members (Fig. 10) occurred at similar locations as in eccentrically loaded columns (Fig. 4), confirming the conclusion that the initial load eccentricities in the tests had very minor effects on the failure modes of specimens.

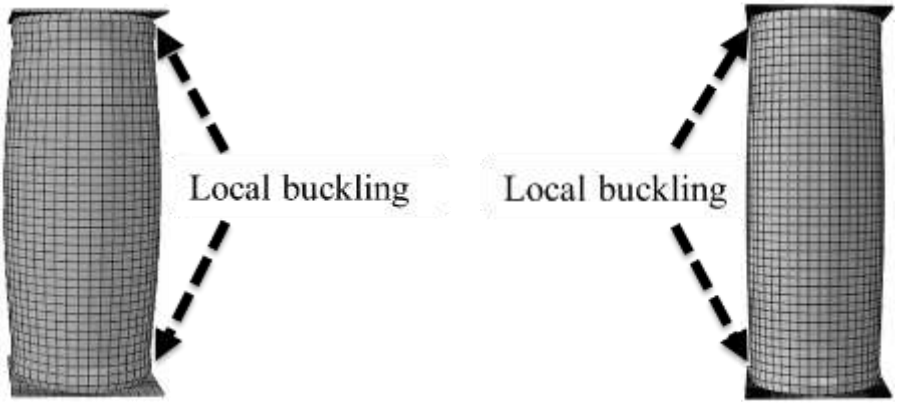

(a) 304-D500-t8c40 specimen (b) 2205-D500-t8c40 specimen

Fig. 10 Typical failure modes of FE models under concentric loading

Comparisons between the test ultimate loads $N_{u,e}$ and the corresponding FE values $N_{u,FE}$ are given in Table 3. It is worth noting that the maximum load of the columns can be considerable, but the corresponding deformation would be too large and unrealistic in practical engineering. To this end, the ultimate loads achieved in the 304 and 2205 CFSST specimens were defined as the loads corresponding to end-shortening strain $\varepsilon_0 = \Delta/L$ of 5% and 2%, where Δ and L are the end-shortening and length of the specimens, respectively. The 5% strain for 304 specimens was defined according to a previous study [12] where the results showed that the 304 CFSST specimens generally reached their ultimate loads at end-shortenings approximately 5% of the specimen length or less. This value (5% strain) was therefore adopted in the current research to facilitate the derivation of ultimate loads from the tests (especially in those where ultimate loads have not been achieved due to the stroke limit of the test machine). Although further increase of load with deformation is possible, it is considered to be unrealistic in engineering practice. Therefore it is defined herein that the load corresponding to 5% strain is the ultimate load of 304 CFSST specimens. For the 2205 specimens,

the same logic applied. However, there is no relevant research on 2205 CFSST specimens. Since the load vs end-shortening curves of 2205 specimens tend to present very slight strain hardening in the plastic stage, therefore the loads at 2% strain are deemed to be representative for their ultimate capacities. For the cases in which the peak load occurred before reaching the specified ε_0, the peak load was adopted as the ultimate load. The average error between the experimental and FE resistances of the austenitic members is 4.5%, and that of the duplex members is 4.9%, as shown in Table 3. Overall, good agreements between the test and finite element results on the part of the failure mode, load vs end-shortening relationship, and ultimate load confirm the validity of the FE models.

4. Parametric study

4.1 Introduction

To study the influences of different parameters (thickness of the stainless tube, cube compressive strength of concrete) on the load-deformation relationships of CFSST columns under axial compression, and to generate a wider range of data pool, a series of parametric analyses were conducted based on the FE models validated in section 3. The related material properties adopted elastic moduli of E_a=1.93×10^5 MPa and E_d = 2.00 × 10^5 MPa, and 0.2% proof stresses of $f_{0.2,a}$ = 205 MPa and $f_{0.2,d}$ = 450 MPa for the austenitic and duplex stainless steels, respectively, where the subscripts 'a' denotes 'austenitic' and 'd' denotes 'duplex'. The varying parameters included three outer diameters (D = 300, 400, 500 mm), two steel grades (austenitic and duplex), and three thicknesses (t = 8, 10, 12, 14, 16, 18 mm) of the stainless steel tubes, and six strengths of the concrete (f_{cu} = 40, 45, 50, 55, 60, 70 MPa), resulting in a total of 216 FE simulations performed.

4.2 Influence of stainless steel tube thickness

Fig. 11 shows typical normalized load-axial deformation relationships of CFSST FE models with varying tube thicknesses, where the results of the specimens with f_{cu} = 55 MPa and D = 300 mm are

plotted. It can be found from Fig. 11 that as t increases from 8mm to 18mm, the normalized bearing capacities of CFSST specimens increase significantly in terms of both the yielding load and the ultimate load. Both the austenitic and duplex specimens have reached yield loads higher than their plastic reference resistances $f_{0.2}A_s + f_{cu}A_c$ and displayed strain hardening beyond yielding. These are attributed to the combined effects of the strain-hardening behavior of the stainless steel materials, the stocky tubular geometries and the confinement of the tube on the concrete. It is worth noticing that the hardening slope is less significant in the duplex CFSST columns than in the austenitic ones. Overall it can be concluded that reducing tube slenderness has a positive contribution to the compressive resistance of CFSST stub columns.

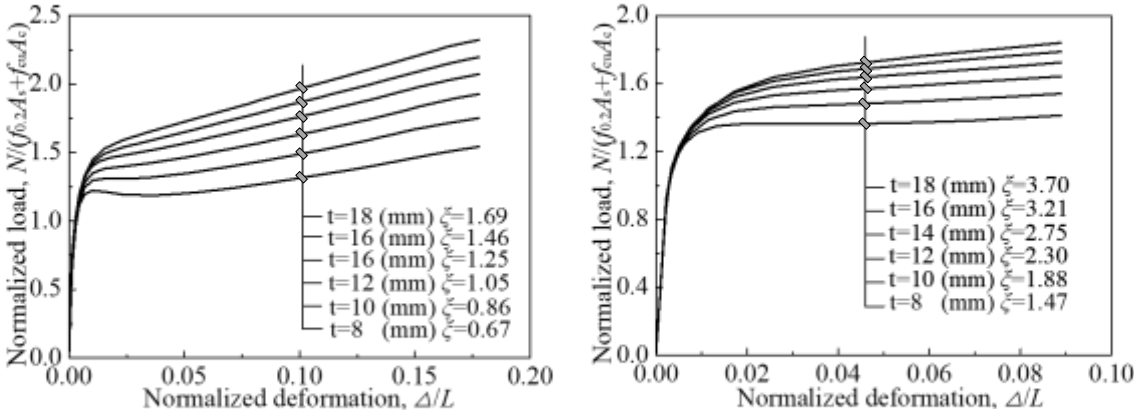

(a) 304 c55-D300 CFSST stub columns (b) 2205 c55-D300 CFSST stub columns

Fig. 11 Normalized load-axial deformation curves of CFSST columns with varying thicknesses

4.3 Influence of concrete strength

To illustrate the contribution strength of concrete to the carrying capacity of CFSST stub columns, the normalized load-axial deformation curves of 304 and 2205 t12-D500 CFSST specimens are plotted in Figs. 12(a) and (b), respectively. It can be seen that increasing the concrete strength leads to a reduced normalized load-carrying capacity. This can be explained by comparisons based on un-normalized load-axial displacement relationships, as given in Fig. 13, where it shows that the concrete contribution to load enhancement is limited, especially at the later stage of loading. This is

because at yielding (first change of slope in the load-displacement relationship) the concrete at the buckling position of steel tube has already broken, leading to very minimal contribution of concrete to the strain hardening response afterwards. Although an increase of the concrete strength is shown to strengthen slightly the resistance of CFSST stub columns at yielding, its effectiveness in increasing the ultimate bearing capacity is not as pronounced as reducing the tube slenderness.

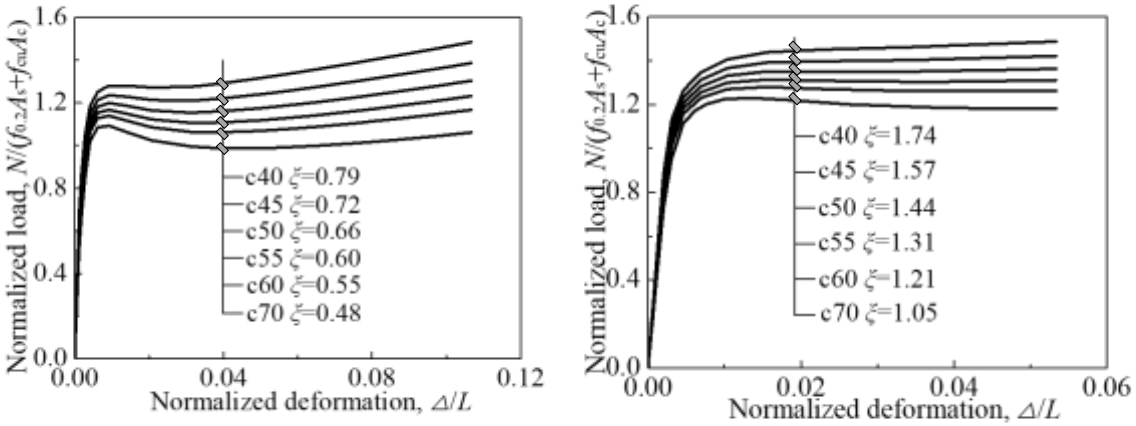

(a) 304 t12-D500 CFSST stub columns (b) 2205 t12-D500 CFSST stub columns

Fig. 12 Normalized load-axial deformation curves of CFSST columns with varying concrete strengths

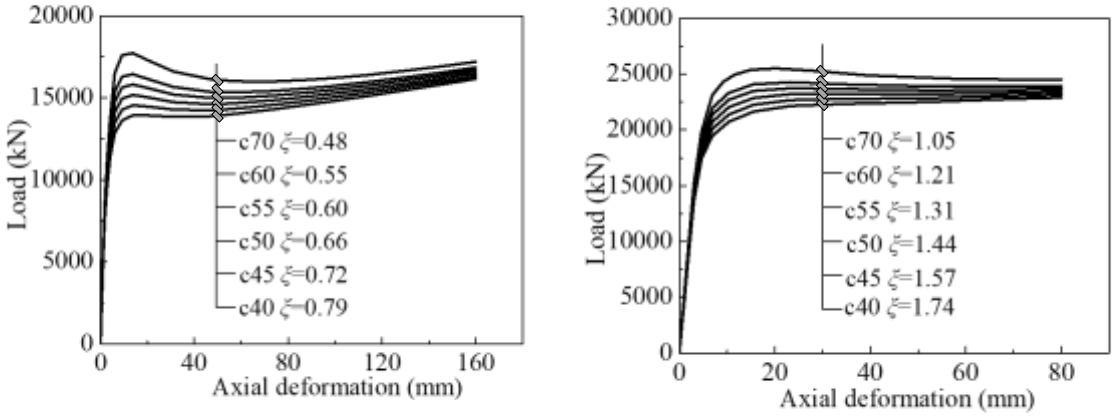

(a) 304 t12-D500 CFSST stub columns (b) 2205 t12-D500 CFSST stub columns

Fig.13 Load-axial deformation curves of CFSST columns with varying concrete strengths

4.4 Influence of confinement factor ξ

The ξ reflects the constraint of the stainless steel tube to the concrete core and its value is given at

the end of each curve for corresponding specimens in Figs. 11, 12 and 14. It can be seen that increased confinement factors is associated with increased normalized resistance and more and more pronounced strain hardening response. This indicates that the confinement factor should play a significant role in the characterization of the steel and concrete composite action when designing the calculation methods for CFSST members. It has also been observed that there is no descent in the load-axial displacement curve for specimens with confinement factors larger than approximately 0.8.

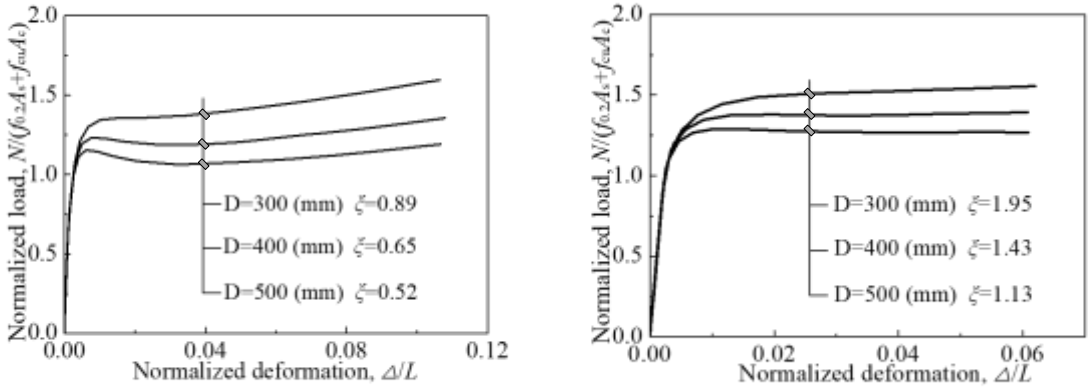

(a) 304 t8c40 CFSST stub columns (b) 2205 t8c40 CFSST stub columns

Fig. 14 Normalized load-axial deformation curves of CFSST columns with varying tube diameters

5. Calculation methods for strength of CFSST stub columns

5.1 Introduction

Currently there are no codified calculation rules available for CFSST members, and to facilitate their design, rules for conventional CFST members may be applied; these include the EN 1994-1-1 [39] adopted in Europe, ACI 318 [35] in North America, AIJ-CFT [40] in Japan and DBJ/T 13-51-2010 [41] and GB 50936-2014 [42] in China. Among these standards, ACI 318 [35] and AIJ-CFT [40] do not consider the composite action between the steel tube and the concrete; DBJ/T 13-51-2010 [41] includes this effect but characterizes it with a very complicated formulation that may be impractical to be used by designers. The EN 1994-1-1 [39] and GB 50936-2014 [42] are the only ones that

consider the strength enhancement brought by the steel-concrete composite action and characterize this effect with relatively straight forward equations. Therefore the EN 1994-1-1 [39] and GB 50936-2014 [42] formulations are employed in the current study to be applied to the design of CFSST members. The specified CFST calculation methods in EN 1994-1-1 [39] and GB 50936-2014 [42] were first compared to the CFSST results obtained in this study, based on which, modifications of algebraic parameters were proposed to give a closer estimation of the CFSST data.

The comparisons in this section were mainly based on the numerical results of perfectly concentrically loaded CFSST stub columns, with all the material strength factors and safety factors set to unity.

5.2 GB 50936-2014

The code of GB 50936-2014 [42] predicts the ultimate resistance of CFST columns by employing the unified theory of considering the steel-concrete composite members as one 'material'. The GB 50936-2014 [42] calculation equation for the cross-section resistance of CFST members under compression is given in Eq. (7):

$$N_{GB} = (1.212 + B\xi + C\xi^2) f_{ck} A_{sc} \quad (7)$$

where N_{GB} is the ultimate resistance under axial compression; A_{sc} is the cross-sectional area of the composite member; $\xi = A_s f_{0.2}/A_c f_{ck}$ is the confinement factor, $B = 0.176 f_{0.2}/213+0.974$ and $C = -0.104 f_{ck}/14.4+0.031$ are the algebraic factors.

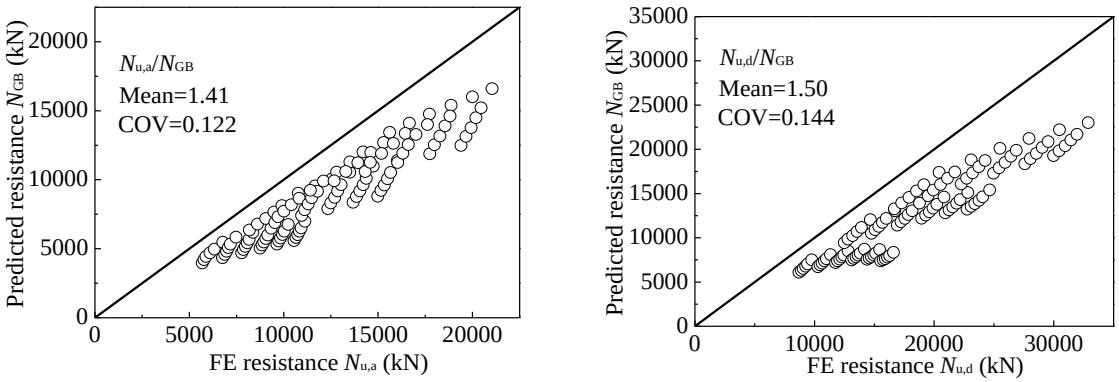

(a) 304 CFSST (b) 2205 CFSST

Fig.15 Comparisons between the FE resistances of CFSST stub columns with the GB 50936-2014 predictions

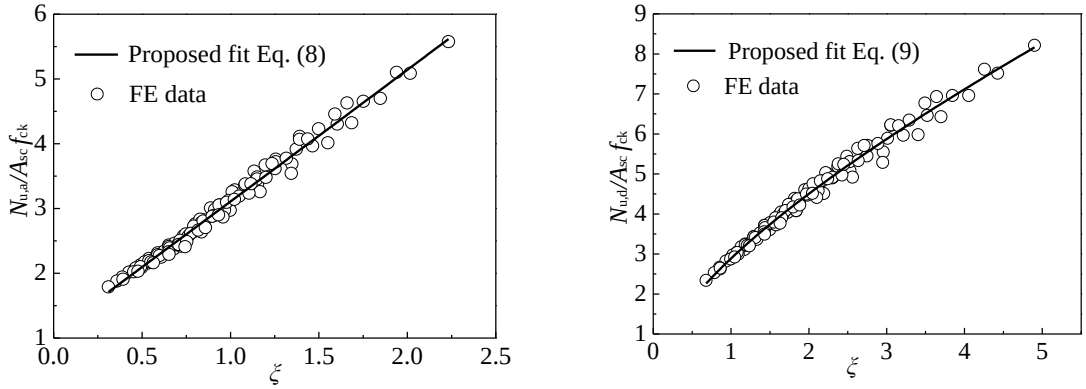

(a) 304 CFSST (b) 2205 CFSST

Fig.16 Normalized resistances $N_u/A_{sc}f_{ck}$ of CFSST stub columns varying with the concrete refinement factor ξ and proposed algebraic characterizations

Comparisons between the FE ultimate resistances of CFSST stub columns and the corresponding GB 50936-2014 predictions are shown in Figs. 15(a) and (b) for the austenitic and duplex CFSST columns, respectively. It can be seen that the current GB 50936-2014 design formulae (Eq. (7)) underestimates both the austenitic and duplex CFSST results significantly, which may be large as a result of the fact that the significant strain-hardening behavior of stainless steel materials is not taken into account.

Based on the GB 50936-2014 formulation (Eq. (7)), modified characterizations as in Eqs. (8) and

(9) are proposed herein for the calculation of austenitic and duplex CFSST members, respectively. Different from Eq. (7), Eqs. (8) and (9) algebraically relate the strength amplification factor (quadratic equation inside the brackets) to the confinement factor ξ only, and release its dependency on $f_{0.2}$ and f_{ck} through the definitions of B and C, which greatly reduces the complexity of the characterization. The validity of Eqs. (8) and (9) can be confirmed by Fig. 16, where the normalized CFSST resistances $N_u/A_{sc}f_{ck}$ display a clear dependency on ξ for both the austenitic and duplex specimens despite the various geometric and material properties being considered. The proposals of Eqs. (8) and (9) were achieved by regression analyses, closely aligning with the trends of the austenitic and duplex CFSST data, as shown in Figs. 16(a) and (b), respectively.

$$N_{u,a} = (1.09 + 2.02\xi + 0.0059\xi^2) f_{ck} A_{sc} \quad (8)$$

$$N_{u,d} = (-0.23 + 2.56\sqrt{\xi} + 0.56\xi) f_{ck} A_{sc} \quad (9)$$

where $N_{u,a}$ and $N_{u,d}$ are the ultimate resistances of austenitic and duplex CFSST columns, respectively.

5.3 EN 1994-1-1

The EN 1994-1-1 compressive strength of concrete-filled circular steel tube columns is given in Eq. (10), which takes the steel-concrete composite action into account through two factors η_s and η_s, as defined by Eqs. (11) and (12), respectively:

$$N_{EC4} = \eta_s A_s f_y + A_c f_c' (1 + \eta_c \frac{t}{D} \frac{f_y}{f_c'}) \quad (10)$$

$$\eta_s = 0.25(3 + 2\bar{\lambda}) \quad (\text{but} \le 1.0) \quad (11)$$

$$\eta_c = 4.9 - 18.5\bar{\lambda} + 17\bar{\lambda}^2 \quad (\text{but} \ge 0) \quad (12)$$

where f_y is yield strength of the steel; f_c' is the cylinder compressive strength of the concrete; $\bar{\lambda}$ is the relative slenderness given by Eq. (13):

$$\bar{\lambda} = \sqrt{\frac{A_s f_y + A_c f_c'}{N_{cr}}} \quad (13)$$

where N_{cr} is the elastic critical normal force for relevant buckling mode (in this paper this

corresponds to the first global flexural buckling mode of the composite column), calculated with the effective flexural stiffness $(EI)_{eff}$ as defined in EN 1994-1-1 [39].

Figs. 17(a) and (b) compare the predicted resistances of CFSST stub columns using the EN 1994-1-1 calculation method (Eqs. (10) - (13)) with the corresponding FE values for the austenitic and duplex specimens, respectively. In general EN 1994-1-1 is shown in Fig. 17 to provide slightly improved predictions compared to GB 50936-2014 in Fig. 15, but is still significantly conservative with approximately 30% over-predictions for both steel grades.

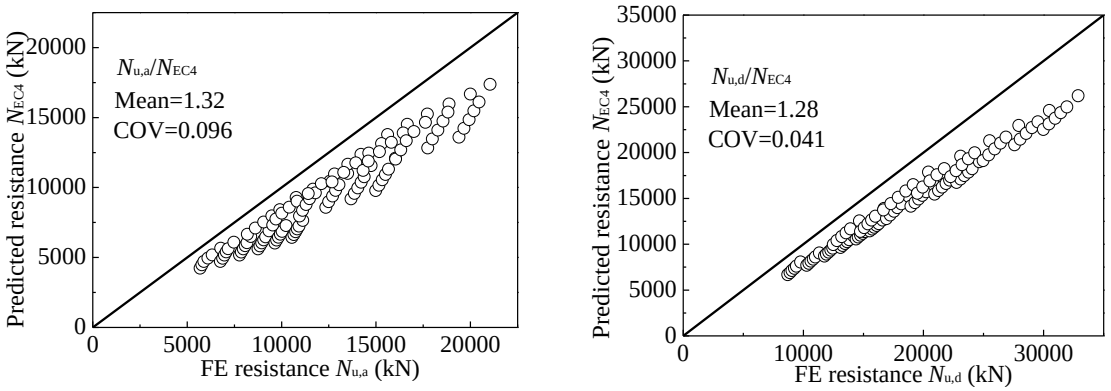

(a) 304 CFSST (b) 2205 CFSST

Fig.17 Comparisons between FE resistances of CFSST stub columns with the EN 1994-1-1 predictions

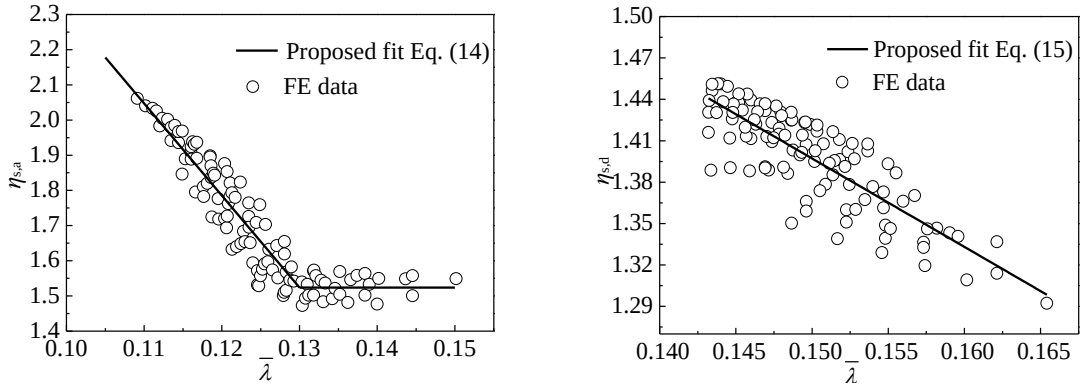

(a) 304 CFSST (b) 2205 CFSST

Fig.18 Back calculated η_s parameters based on the CFSST stub column results varying with the dimensionless member slenderness $\bar{\lambda}$ and proposed algebraic characterizations

To provide a closer estimation of the ultimate resistances of CFSST members, modifications to the EN 1994-1-1 calculation method are proposed in this study, maintaining the basic formulation of Eq. (10) with an updated η_s parameter to account for the change of steel material from carbon steel to stainless steel. The back calculated η_s values based on the computed ultimate resistances $N_{u,a}$ and $N_{u,d}$ are plotted against $\bar{\lambda}$ in Figs. 18(a) and (b) for the austenitic and duplex CFSST members, respectively. Eqs. (14) and (15) were then achieved through regression analyses, providing good estimations of the η_s - $\bar{\lambda}$ relationships for the two steel grades, as also being plotted in Figs. 18(a) and (b), respectively.

$$\eta_{s,a} = \begin{cases} 4.924 - 26.155\bar{\lambda} & (\bar{\lambda} \le 0.132) \\ 1.472 & (\bar{\lambda} > 0.132) \end{cases} \quad (14)$$

$$\eta_{s,d} = 2.358\text{-}6.409\bar{\lambda} \quad (15)$$

where $\eta_{s,a}$ and $\eta_{s,d}$ are the updated η_s factors for the austenitic and duplex CFSST members, respectively.

6. Conclusions

An experimental and numerical study of the compressive behavior of CFSST stub columns has been carried out. Nine austenitic and nine duplex CFSST columns were tested and FE models were established to duplicate the experiments. Based on the validated FE models, parametric analyses were conducted to consider a wider range of geometric and material properties. The conclusions drawn from the current study include:

- All the tested austenitic and duplex CFSST columns presented the local buckling of the stainless tube as their failure modes. The percentage end-shortenings at failure for the austenitic CFSST columns were significantly larger than those of the duplex CFSST columns.
- The load vs end-shortening relationships showed that CFSST columns possess high deformability after entering the plastic stage. While the austenitic CFSST specimens displayed

the significant strain-hardening response, the duplex CFSST specimens showed a slightly declining trend of the load-bearing capacity. It should be noted that yield strain has been reached in all specimens before the peak load was attained, demonstrating a positive tube-concrete interaction.

- The slenderness of the stainless steel tube has a higher influence on the load-bearing capacity of CFSST members than the concrete strength.
- The concrete confinement factor ξ was shown directly related to the normalized resistance $N_u/A_{sc}f_{ck}$ of CFSST columns, based on which, modifications to the current GB 50936-2014 calculation methods have been made to estimate the ultimate resistance of CFSST columns.
- Based on the obtained FE data, modifications to the current EN 1994-1-1 calculation methods have also been made by updating the steel contribution factor η_s.

Acknowledgements

This work was supported by the Beijing Excellent Talent Training Support (Grant No. 2017000026833ZK26), the Foundation for Innovative Research Groups of the National Natural Science Foundation of China (Grant No. 51421005).

References

[1] Y. Ye, L.H. Han, Z.X. Guo, Concrete-filled bimetallic tubes (CFBT) under axial compression: Analytical behavior, Thin-Walled Struct. 119 (2017) 839-850.

[2] L. Zhu, L. Ma, Y. Bai, et al., Large diameter concrete-filled high strength steel tubular stub columns under compression, Thin-Walled Struct. 108 (2016) 12–19.

[3] Z.B. Wang, Z. Tao, Q.Yu, Axial compressive behaviour of concrete-filled double-tube stub columns with stiffeners, Thin-Walled Struct. 120 (2017) 91-104.

[4] M. Shams, M.A. Saadeghvaziri, State of the art of concrete-filled steel tubular columns, Aci Struct. J. 94 (5) (1997) 558-571.

[5] Z. Tao, B. Uy, L.H. Han, Z.B. Wang, Analysis and design of concrete-filled stiffened thin-

422 walled steel tubular columns under axial compression, Thin-Walled Struct. 47 (12) (2009)
423 1544-1556.
424 [6] B. Lakshmi, N.E. Shanmugam, Nonlinear Analysis of In-Filled Steel-Concrete Composite
425 Columns, J. Struct. Eng. ASCE 128 (7) (2002) 922-933.
426 [7] H.T. Hu, C.S. Huang, M.H. Wu, Y.M. Wu, Nonlinear Analysis of Axially Loaded Concrete-
427 Filled Tube Columns with Confinement Effect, J. Struct. Eng. ASCE 129 (10) (2003) 1322-
428 1329.
429 [8] K. Sakino, H. Nakahara, S. Morino, Behavior of Centrally Loaded Concrete-Filled Steel-Tube
430 Short Columns, J. Struct. Eng. ASCE 130 (2) (2004) 180-188.
431 [9] T. Fujimoto, A. Mukai, I. Nishiyama, Sakino K, Behavior of Eccentrically Loaded Concrete-
432 Filled Steel Tubular Columns, J. Struct. Eng. ASCE 130 (2) (2004) 203-212.
433 [10] M. Dundu, Compressive strength of circular concrete filled steel tube columns, Thin-Walled
434 Struct. 56 (2012) 62-70.
435 [11] L.H. Han, C.Y. Xu, Z. Tao, Performance of concrete filled stainless steel tubular (CFSST)
436 columns and joints: Summary of recent research, J. Constr. Steel Res. 152 (2019) 117-131.
437 [12] D. Lam, L. Gardner, Structural design of stainless steel concrete filled columns, J. Constr. Steel
438 Res. 64 (11) (2008) 1275-1282.
439 [13] B. Young, E. Ellobody, Experimental investigation of concrete-filled cold-formed high
440 strength stainless steel tube columns, J. Constr. Steel Res. 62 (5) (2006) 484-492.
441 [14] M.A. Dabaon, M.H. El-Boghdadi, M.F. Hassanein, Experimental investigation on concrete-
442 filled stainless steel stiffened tubular stub columns, Eng. Struct. 31 (2) (2009) 300-307.
443 [15] Z. Tao, B. Uy, F.Y. Liao, L.H. Han, Nonlinear analysis of concrete-filled square stainless steel
444 stub columns under axial compression, J. Constr. Steel Res. 67 (11) (2011) 1719-1732.
445 [16] B. Uy, Z. Tao, L.H. Han, Behavior of short and slender concrete-filled stainless steel tubular
446 columns, J. Constr. Steel Res. 67 (3) (2011) 360-378.
447 [17] A. He, F.Y. Wang, O. Zhao, Experimental and numerical studies of concrete-filled high-
448 chromium stainless steel tube (CFHSST) stub columns, Thin-Walled Struct. 144 (2019) 106273.
449 [18] Y. Chen, R. Feng, Y. Shao, X. Zhang, Bond-slip behavior of concrete-filled stainless steel
450 circular hollow section tubes, J. Constr. Steel Res. 130 (2017) 248-263.
451 [19] Y. Chen, R. Feng, L. Wang, Flexural behavior of concrete-filled stainless steel SHS and RHS
452 tubes, Eng. Struct. 134 (2017) 159-171.

[20] E. Ellobody, A consistent nonlinear approach for analysing steel, cold-formed steel, stainless steel and composite columns at ambient and fire conditions, Thin-Walled Struct. 68 (2013) 1-17.
[21] EN 1992-1-1, Eurocode 2, design of concrete structures – part 1-1: general rules and rules for buildings, CEN, Brussels, 2004.
[22] Y. Ye, S.J. Zhang, L.H. Han, Y. Liu, Square concrete-filled stainless steel/carbon steel bimetallic tubular stub columns under axial compression, J. Constr. Steel Res. 146 (2018) 49-62.
[23] BS EN ISO 6892-1:2009, Metallic materials - tensile testing part 1: method of test at ambient temperature, The Standards Policy and Strategy Committee, 2009.
[24] EN 1993-1-4, Eurocode 3, design of steel Structures - part 1-4: general rules: supplementary rules for stainless steels, CEN, 2015.
[25] GB/T 50081-2002, Standard for test method of mechanical properties on ordinary concrete, Beijing, 2003 (In Chinese).
[26] Y.F. Yang, L.H. Han, Experimental behavior of recycled aggregate concrete filled stainless steel tube stub columns and beams, J. Constr. Steel Res. 62 (12) (2006) 1310-1324.
[27] Z. Tao, Z.B. Wang, Q. Yu, Finite element modelling of concrete-filled steel stub columns under axial compression, J. Constr. Steel Res. 89 (5) (2013) 121-131.
[28] W. Ramberg, W.R. Osgood, Description of stress-strain curves by three parameters, NACA Technical Note, No. 902, 1943.
[29] E. Mirambell, E. Real, On the calculation of deflections in structural stainless steel beams: an experimental and numerical investigation, J. Constr. Steel Res. 54 (1) (2000) 109-133.
[30] K.J.R. Rasmussen, Full-range stress–strain curves for stainless steel alloys, J. Constr. Steel Res. 59 (1) (2003) 47-61.
[31] T.S. Kim, H. Kuwamura, Finite element modeling of bolted connections in thin-walled stainless steel plates under static shear, Thin-Walled Struct. 45 (4) (2007) 407-421.
[32] F.C. Wang, L.H. Han, W. L, Analytical behavior of CFDST stub columns with external stainless steel tubes under axial compression, Thin-Walled Struct. 127 (2018) 756–768.
[33] J.B.P. Lim, D.A. Nethercot, Stiffness prediction for bolted moment connections between cold-formed steel members, J. Constr. Steel Res. 60 (1) (2004) 85–107.
[34] L.H. Han, G.H. Yao, Z. Tao, Performance of concrete-filled thin-walled steel tubes under pure

torsion, Thin-Walled Struct. 45 (1) (2007) 24-36.
[35] ACI 318, Building code requirements for structural concrete, American Concrete Institute, Detroit (MI), 2002.
[36] GB 50010-2010, Code for design of concrete structures, Ministry of Housing and Urban-Rural Development of the People's Republic of China, Beijing, 2010 (In Chinese).
[37] S.P. Schneider, Axially loaded concrete-filled steel tubes, J. Struct. Eng. ASCE 124 (10) (1998) 1125–1138.
[38] K.A.S. Susantha, H. Ge, T. Usami, Uniaxial stress–strain relationship of concrete confined by various shaped steel tubes, Eng. Struct. 23 (10) (2001) 1331-1347.
[39] Eurocode 4, Design of composite steel and concrete structures. Part 1-1: General rules and rules for building. Brussels: EN 1994-1-1:2004, European Committee for Standardization, 2004.
[40] AIJ-CFT, Recommendations for design and construction of concrete filled steel tubular structures, Architectural Institute of Japan, 1997.
[41] DBJ/T 13-51-2010, Technical specification for concrete-filled steel tubular structures, The Construction Department of Fujian Province, Fuzhou (China), 2010 (in Chinese).
[42] GB 50936-2014, Technical code for concrete filled steel tubular structures, Ministry of Housing and Urban-Rural Development of the People's Republic of China, Beijing (China), 2014 (in Chinese).

503 ***Notations***

A_c	cross-sectional areas of concrete core
A_s	cross-sectional areas of stainless steel tube
A_{sc}	cross-sectional area of composite member
D	outer diameter of stainless steel tube
E_c	modulus of elasticity of concrete
E_0	Young's modulus of stainless steel
$E_{0.2}$	tangent elastic modulus when stress reaches $\sigma_{0.2}$
$f_{0.2}$	0.2% proof stress of stainless steel (= $\sigma_{0.2}$)
f_{b0}	compressive strength of concrete under biaxial loading
f_{ck}	characteristic compressive strength of concrete
f_{cu}	cube compressive strength of concrete
$f_{cu,\,100}$	cube compressive strength obtained from 100 mm concrete cube test
f_u	ultimate stress of stainless steel (=σ_u)
f_c'	cylinder compressive strength of concrete
L	length of stainless steel tube
n	Ramberg-Osgood strain hardening exponent
N	axial load
N_{cr}	elastic critical normal force
N_{GB}	ultimate resistance calculated by code of GB 50936-2014
N_{EC4}	ultimate resistance calculated by Eurocode 4
$N_{u,e}$	ultimate load obtained from experiments
$N_{u,FE}$	ultimate load obtained from FE models
t	thickness of stainless steel tube
ε	strain
ε_f	plastic strain at fracture
ε_{nom}	constructed engineering strain
ε_{true}	true strain
ε_u	strain at ultimate tensile stress
$\bar{\lambda}$	relative slenderness
ν	Poisson's ratio
ξ	concrete confinement factor
σ	stress
$\sigma_{0.01}$	measured 0.01% proof stress
σ_{nom}	constructed engineering stress
σ_{true}	true stress

504